Electronic Supplementary Information for:

Three-dimensional Solid Additive Suppresses Non-Radiative Recombination Loss to Boost Efficiency and Scalability in Organic Photovoltaics

Zhongjie Li,[a] Lingling Zhan,[*a] Huayu Qiu,[a] Xiaokang Sun,[c] Hanlin Hu,[c] Ruohua Gui,[d] Hang Yin,[d] Rui Sun,[e] Jie Min,[e] Jinyang Yu,[b] Weifei Fu,[b] Weiming Qiu,[f] Zhi-Xi Liu,[*b,g] Shouchun Yin,[*a] and Hongzheng Chen[*b]

[a.] Key Laboratory of Organosilicon Chemistry and Materials Technology of Ministry of Education, College of Materials, Chemistry and Chemical Engineering, Hangzhou Normal University, Hangzhou 311121, P. R. China. E-mail: linglingzhan@hznu.edu.cn; yinsc@hznu.edu.cn
[b.] State Key Laboratory of Silicon and Advanced Semiconductor Materials, Department of Polymer Science and Engineering, Zhejiang University, Hangzhou 310027, P. R. China. E-mail: z-xliu@zju.edu.cn; hzchen@zju.edu.cn
[c.] Hoffmann Institute of Advanced Materials, Shenzhen Polytechnic University, 518055 Shenzhen, P. R. China
[d.] School of Physics, Shandong University, Jinan, 250100, P. R. China
[e.] The Institute for Advanced Studies, Wuhan University, Wuhan 430072, P. R. China
[f.] Guangzhou Chasinglight Technology Co., Ltd, Guangzhou 510535, P. R. China.
[g.] Zhejiang University-Hangzhou Global Scientific and Technological Innovation Center, Hangzhou 311200, P.R. China.

Materials and Methods

Instrument.

Cyclic voltammetry (CV) was done on a CHI600A electrochemical workstation with Pt disk, Pt plate, and standard calomel electrode (SCE) as working electrode, counter electrode, and reference electrode, respectively, in a 0.1 mol L^{-1} tetrabutylammonium hexafluorophosphate (Bu_4NPF_6) acetonitrile solution. The CV curves were recorded versus the potential of SCE, which was calibrated by the ferrocene-ferrocenium (Fc/Fc^+) redox couple (4.8 eV below the vacuum level). The equation of $E_{LUMO/HOMO} = -e(E_{red/ox}+4.41)$ (eV) was used to calculate the LUMO and HOMO levels (the redox potential of Fc/Fc^+ is found to be 0.39 V).

UV-Vis absorption spectra were recorded on a Shimadzu UV-1800 spectrophotometer. The pumping light wavelength used to excite the samples was 750 nm, with a power of 10 mW.

Topographic images of the films were obtained on a Veeco MultiMode **atomic force microscopy (AFM)** in the tapping mode using an etched silicon cantilever at a nominal load of ~2 nN, and the scanning rate for a 10 μm×10 μm image size was 1.5 Hz.

GIWAXS measurements were carried out with a Xeuss 2.0 SAXS/WAXS laboratory beamline using a Cu X-ray source (8.05 keV, 1.54 Å) and a Pilatus3R 300K detector. The incidence angle is 0.2º.

The *J-V* measurement was performed via the solar simulator (SS-F5-3A, Enlitech) along with AM 1.5G spectra whose intensity was calibrated by the certified standard silicon solar cell (SRC-2020, Enlitech) at 100 mW cm^{-2}. The external quantum efficiency (EQE) data were obtained by using the solar-cell spectral-response measurement system (RE-R, Enlitech).

Light Stability tests were taken for encapsulated devices under 1 sun illumination in ambient conditions under room temperature (stability measurement system equipped with cooling plant), and storage stability in the nitrogen-atmosphere glove box were examined respectively.

For femtosecond **transient absorption (fs-TAS) spectroscopy**, the total output from Yb:KGW laser (1030 nm, 220 fs Gaussian fit, 100 kHz, Light Conversion Ltd) was separated into two light beams. One beam was introduced to NOPA (ORPHEUS-N, Light Conversion Ltd) to produce a specific wavelength for the pump beam (here, we use 800 nm), and the other beam was focused onto a YAG plate to generate a white light continuum as a probe beam. The pump and probe overlapped on the sample at a slight angle of less than 10°. A linear CCD array collected the transmitted probe light from the sample. Samples were kept in a N_2 filled cell at room temperature for all TA measurements.

The charge carrier mobilities of the binary and ternary blend films were measured using the **space-charge-limited current (SCLC)** method. Hole-only devices were fabricated in a structure of indium tin oxide (ITO)/PEDOT:PSS/active layer/MoO_3/Ag. Electron-only devices were fabricated in a structure of ITO/ZnO/active layer/PFN-Br/Al. The device characteristics were extracted by modeling the dark current under forward bias using the SCLC expression described by the Mott-Gurney law:

$$J = \frac{9}{8}\varepsilon_r \varepsilon_0 \mu \frac{V^2}{L^3} \quad (1)$$

Here, $\varepsilon_r \approx 3$ is the average dielectric constant of the blend film, ε_0 is the permittivity of the free space, μ is the carrier mobility, L is the thickness of the film, and V is the applied voltage.

FTPS-EQE measurements were recorded using a Bruker Vertex 70 Fourier-transform infrared (FTIR) spectrometer, equipped with a quartz tungsten halogen lamp, a quartz beam-splitter, and an external detector option. A low noise current amplifier (Femto DLPCA-200) was used to amplify the photocurrent produced on the illumination of the photovoltaic devices with light modulated by FTIR. The output voltage of the current amplifier was fed back into the external detector port of FTIR. The photocurrent spectrum was collected by FTIR's software.

Electroluminescence (EL) quantum efficiency (EQE_{EL}) measurements were performed by applying external voltage sources through the devices from 1V to 4V. A Keithley 2400

SourceMeter was used for supplying voltages and recording injected currents, and a Keithley 485 picoammeter was used for measuring the emitted light intensity.

Energy loss analysis can be quantified as the following formula:

$$\begin{aligned} E_{loss} = E_g - qV_{oc} &= \left(E_g - qV_{oc}^{SQ}\right) + \left(qV_{oc}^{SQ} - qV_{oc}^{rad}\right) + \left(qV_{oc}^{rad} - qV_{oc}\right) \\ &= \left(E_g - qV_{oc}^{SQ}\right) + q\Delta V_{oc}^{rad,below\ gap} + q\Delta V_{oc}^{non-rad} \\ &= \Delta E_1 + \Delta E_2 + \Delta E_3 \qquad (2) \end{aligned}$$

where E_g is the band-gap, V_{oc}^{SQ} is the maximum V_{OC} under the SQ limit, and V_{oc}^{SQ} is the V_{OC} when only radiative recombination is considered.

Materials

All reagents and solvents, unless otherwise specified, were purchased from commercial sources and used without further purification. PM6, Y6, L8-BO, BTP-eC9, DCBB, PDINN were purchased from Solarmer Inc. TPA-DCN (T1), TPA-IC (T2), TPA-NI (T3), TPA-T-NI (T4) and TPA-TA-NI (T5) were synthesized by our group.

Device fabrication and characterization

Organic photovoltaics (OPVs) were fabricated on glass substrates commercially pre-coated with a layer of ITO with the conventional structure of ITO/PEDOT:PSS/active layer/PDINN/Ag. Prior to fabrication, the substrates were cleaned using detergent, deionized water, acetone and isopropanol consecutively for 10 min in each step, and then treated in an ultraviolet ozone generator for 20 min before being spin-coated at 4000 rpm with a layer of 10 nm thick PEDOT:PSS (Baytron P AI4083). After baking the PEDOT:PSS layer in air at 150 ºC for 15 min, the substrates were transferred to a glovebox. For all PM6:Y6-based bulk-heterojunction (BHJ) active layer, the blend film was spin coated from 16.5 mg/mL chloroform solution: the donor/acceptor weight ratio was 1:1.2 and then dissolved in chloroform solution with 0.3% additive of chloronaphthalene (CN) by volume or 5% solid additives of T1~T5 by weight ratio of donor, and stirred at 50 ºC for 3 hours. For layer-by-layer (LBL) active layer:

donor was spin coated from the chloroform solution, with 0%~10% solid additives of T5 by weight ratio of donor, at the concentration of 7 mg/mL at 3000 rpm for 30 s, acceptor as spin coated from the chloroform solution with 0.3% additive of chloronaphthalene (CN) or 3% solid additives of T5 by weight ratio of acceptor, or DCBB with 10 mg/mL concentration, at the concentration of 8 mg/mL at 3000 rpm for 30 s. An extra pre-annealing at 80 ºC for 10 min was performed, and then a 5 nm thick PDINN film was deposited as the cathode buffer layer by the spin-coating of a solution of 1 mg/mL PDINN in methanol. Finally, the Ag (100 nm) electrode was deposited by the thermal evaporation to complete the device with an active area of 6 mm^2, and the testing aperture area is 4.73 mm^2. The thickness of all small area devices is around 100 nm.

To create isolated cell units (P1), the film stack was laser-scribed using a 1064 nm nanosecond laser beam (2 W) on ITO glass substrates measuring 5.5 × 5.5 cm^2. A PEDOT (Heraeus Clevios PVP AI 4083) solution was blade-coated onto the ITO substrates, followed by a thermal annealing process at 150°C for 10 minutes to solidify the layer. The active layer was then deposited from a 14 mg/mL toluene solution (D:A ratio = 1:1.2 w/w, with or without T5 additive) onto a pre-heated substrate at 45°C using a blade-coating speed of 15 mm/s under ambient conditions. This layer was subsequently annealed at 85°C for 10 minutes. Next, a PDINN solution (1 mg/mL in methanol) was applied to the freshly formed BHJ film. Following the completion of the layer stack, P2 scribing was conducted using a 532 nm nanosecond laser beam (2 W) to expose the ITO layer for subsequent electrical connections. Finally, a silver electrode (100 nm) was thermally deposited under reduced pressure, with P3 scribing carried out using the same 532 nm laser to complete the device.

Synthesis route of solid additives

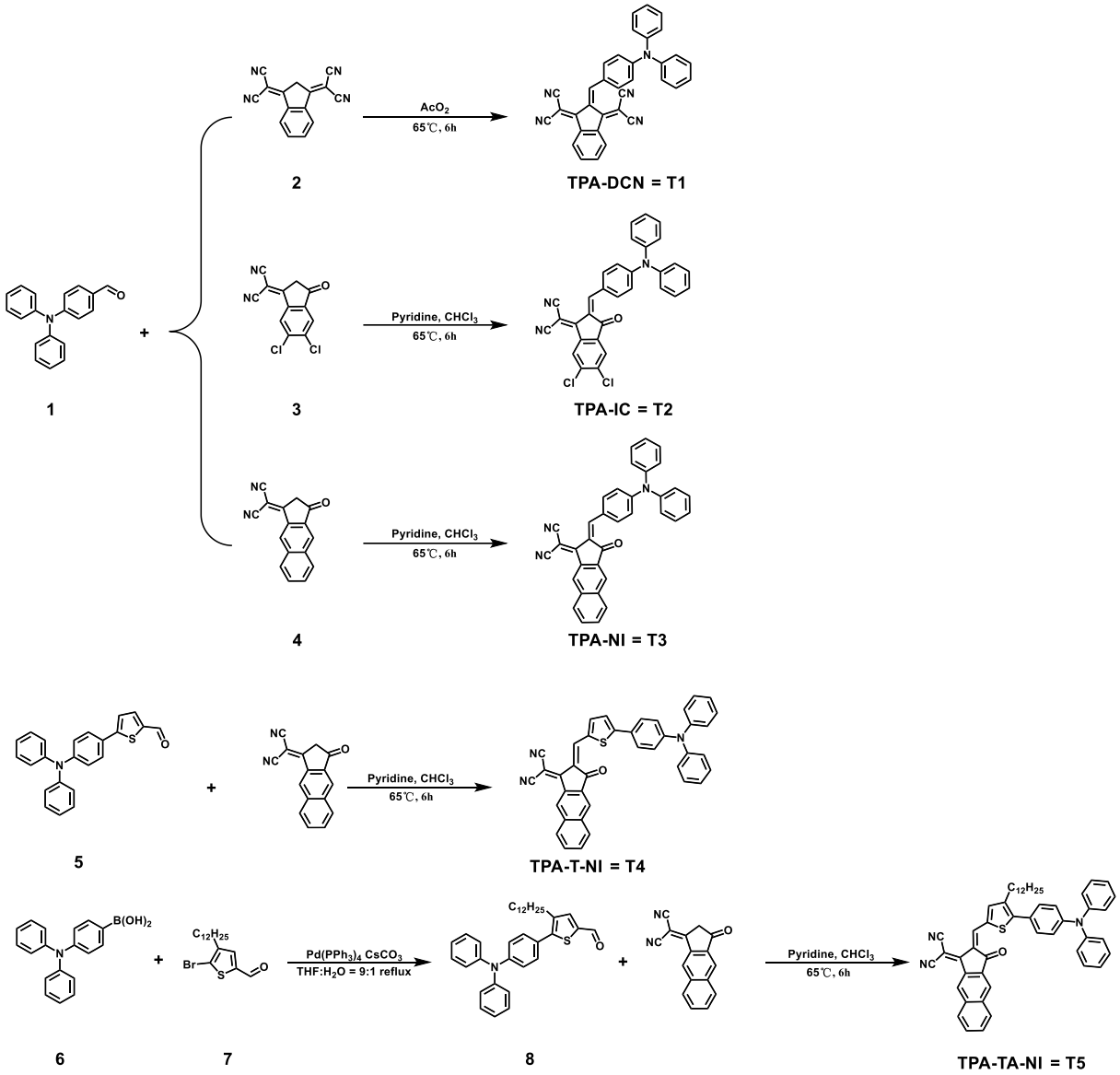

Scheme S1. The synthetic route of T1~T5.

TPA-DCN (T1):

Compound 1 (50 mg, 0.18 mmol) and compound 2 (87 mg, 0.36 mmol) in acetic anhydride (10 mL) were added to a Schlenk tube; Freeze with liquid nitrogen, pump three times, thaw. Under the protection of nitrogen, the reactants were refluxed at 65 ℃ for 6 h. After the reaction was finished, the black solid was obtained, which was further recrystallized from chloroform/*n*-hexane mixture to give the final product T1 (70 mg, 79%). ^{1}H NMR (500 MHz, $CDCl_3$) δ 8.63

(s, 1H), 8.58 (s, 2H), 7.78 (dd, *J* = 5.5, 3.0 Hz, 2H), 7.43 (d, *J* = 8.7 Hz, 2H), 7.38 (t, *J* = 7.6 Hz, 4H), 7.24 (d, *J* = 7.5 Hz, 2H), 7.21 (d, *J* = 7.6 Hz, 4H), 7.00 (d, *J* = 8.7 Hz, 2H).

TPA-IC (T2):

Compound 1 (50 mg, 0.18 mmol) and compound 3 (95 mg, 0.36 mmol) in chloroform (10 mL) were added to a Schlenk tube; Freeze with liquid nitrogen, pump three times, thaw. Under the protection of nitrogen, 0.5 mL of pyridine was injected into the thawed mixing system, and the reactants were refluxed at 65 ℃ for 6 h. After the reaction was finished, the green solid was obtained, which was further recrystallized from chloroform/ethyl alcohol mixture to give the final product T2 (66 mg, 71%). ^{1}H NMR (500 MHz, $CDCl_3$) δ 8.72 (s, 1H), 8.45 (s, 1H), 8.19 (d, *J* = 9.0 Hz, 2H), 7.88 (s, 1H), 7.38 (t, *J* = 7.8 Hz, 4H), 7.24 (s, 2H), 7.21 (d, *J* = 7.6 Hz, 4H), 6.93 (d, *J* = 9.0 Hz, 2H).

TPA-NI (T3):

Compound 1 (50 mg, 0.18 mmol) and compound 4 (88 mg, 0.36 mmol) in chloroform (10 mL) were added to a Schlenk tube; Freeze with liquid nitrogen, pump three times, thaw. Under nitrogen protection, 0.5 mL of pyridine was injected into the thawed mixing system, and the reactants were refluxed at 65 ℃ for 6 h. After the reaction was finished, the bluish cossack green solid was obtained, which was further recrystallized from chloroform/ethyl alcohol mixture to give the final product T3 (79 g, 88%). ^{1}H NMR (500 MHz, $CDCl_3$) δ 9.05 (s, 1H), 8.46 (s, 1H), 8.27 (s, 1H), 8.25 (s, 2H), 7.98 (ddd, *J* = 19.8, 5.8, 3.2 Hz, 2H), 7.64 (dd, *J* = 6.2, 3.1 Hz, 2H), 7.39 (t, *J* = 7.8 Hz, 4H), 7.23 (d, *J* = 8.2 Hz, 6H), 6.96 (d, *J* = 8.9 Hz, 2H).

TPA-T-NI (T4):

Compound 4 (87 mg, 0.36 mmol) and compound 5 (64 mg, 0.18 mmol) in chloroform (10 mL) were added to a Schlenk tube; Freeze with liquid nitrogen, pump three times, thaw. Under nitrogen protection, 0.5 mL of pyridine was injected into the thawed mixing system, and the reactants were refluxed at 65 ℃ for 6 h. After the reaction was finished, the henna solid was obtained, which was further recrystallized from chloroform/n-hexane mixture to give the final product T4 (95 mg, 91%). ^{1}H NMR (500 MHz, $CDCl_3$) δ 9.11 (s, 1H), 8.86 (s, 1H), 8.33 (s, 1H), 8.02 (t, J = 8.3 Hz, 2H), 7.83 (d, J = 4.1 Hz, 1H), 7.67 (s, 1H), 7.66 (s, 1H), 7.66 (s, 1H), 7.64 (s, 1H), 7.39 (d, J = 4.1 Hz, 1H), 7.33 (t, J = 7.8 Hz, 4H), 7.17 (d, J = 7.7 Hz, 4H), 7.14 (s, 1H), 7.13 (s, 1H), 7.05 (d, J = 8.7 Hz, 2H).

TPA-TA-NI (T5):

Compound 6 (88 mg, 0.305 mmol), compound 7 (100 mg, 0.278 mmol), Cs_2CO_3 (181 mg, 0.556 mmol) and Pd $(Ph_3)_4$ (32mg, 0.0278 mmol) in tetrahydrofuran (THF):H_2O = 9:1 (20 mL). The reaction was refluxed at 80 ℃ for 16 h. After the reaction was finished, the orange oily matter was purifed by SiO_2 column (petroleum ether: dichloromethane = 3:1, *v*/*v*). Compound 4 (88 mg, 0.36 mmol) and compound 8 (94 mg, 0.18 mmol) in chloroform (15 mL) were added to a Schlenk tube; Freeze with liquid nitrogen, pump three times, thaw. Under nitrogen protection, 0.5 mL of pyridine was injected into the thawed mixing system, and the reactants were refluxed at 65 ℃ for 6 h. After the reaction was finished, the green solid was obtained. The resulted solid was further recrystallized from chloroform/n-hexane mixture to give the final product T5 (123 mg, 91%). ^{1}H NMR (500 MHz, $CDCl_3$) δ 9.09 (s, 1H), 8.82 (s, 1H), 8.30 (s, 1H), 7.99 (d, J = 8.1 Hz, 2H), 7.71 (s, 1H), 7.68 – 7.63 (m, 2H), 7.44 (d, J = 8.5 Hz, 2H), 7.33 (t, J = 7.7 Hz, 4H), 7.18 (d, J = 7.8 Hz, 4H), 7.14 (s, 1H), 7.12 (s, 1H), 7.11 (s, 1H), 7.09 (s, 1H), 2.74 – 2.69 (m, 2H), 1.65 (dd, J = 14.7, 7.4 Hz, 2H), 1.33 – 1.24 (m, 18H), 0.88 (t, J = 6.8 Hz, 3H).

Supporting Figures

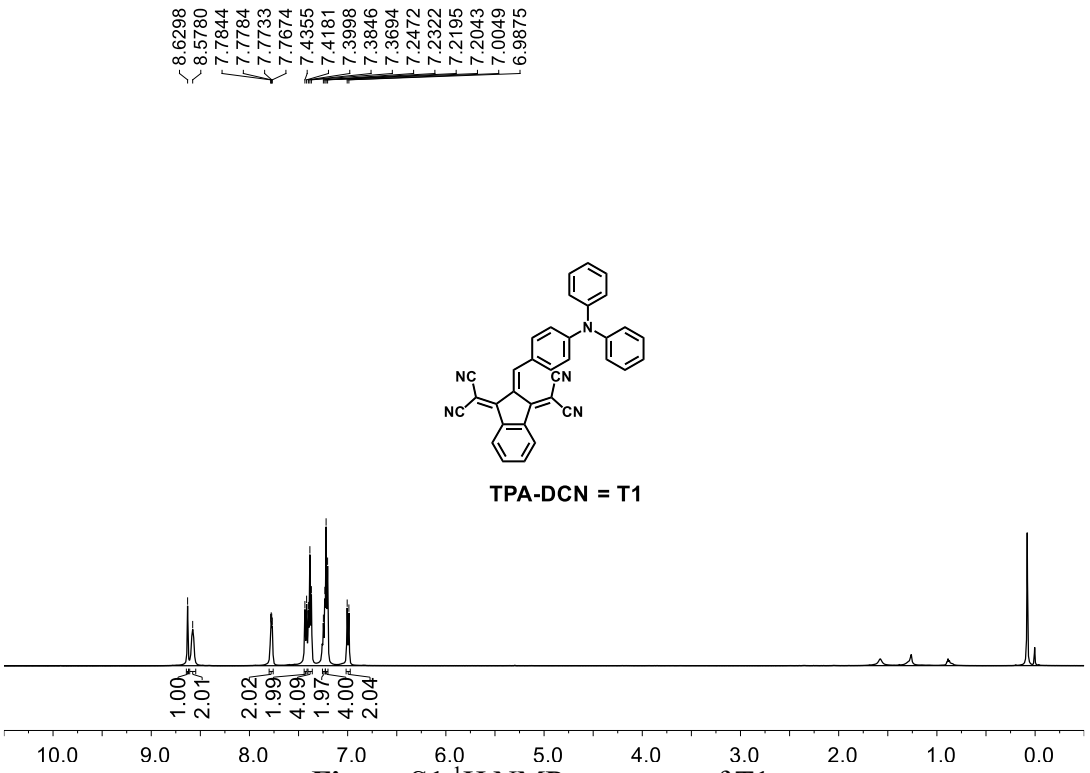

Figure S1 ^{1}H NMR spectrum of T1.

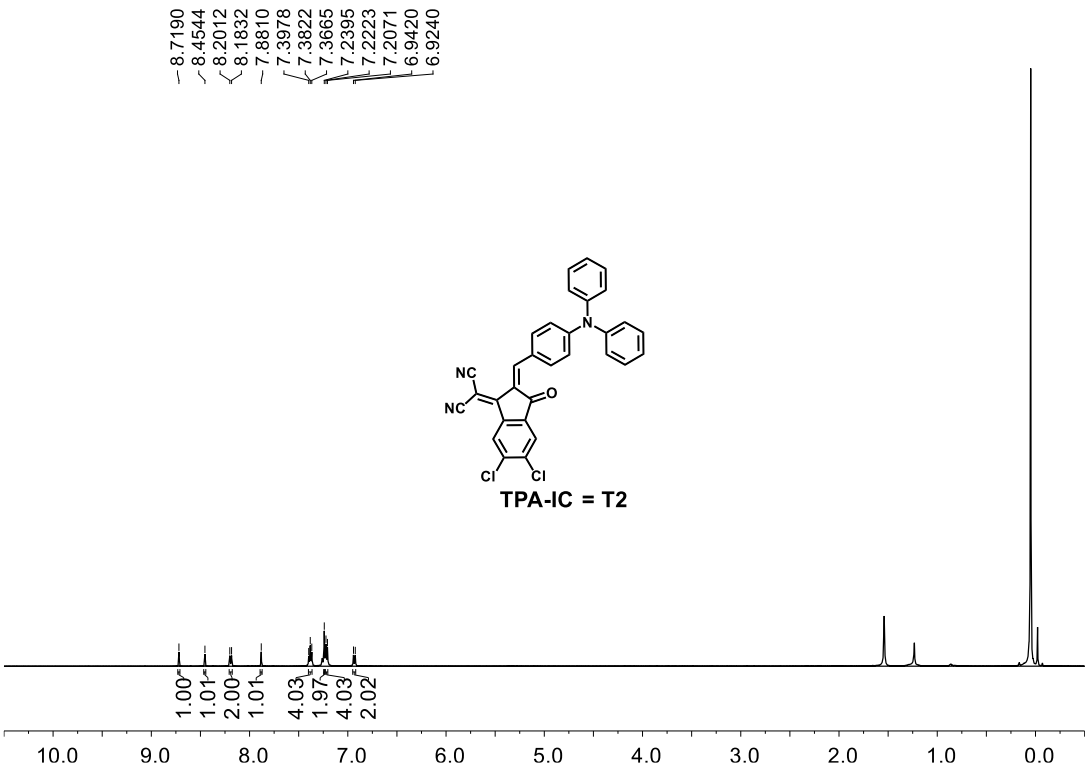

Figure S2 ^{1}H NMR spectrum of T2.

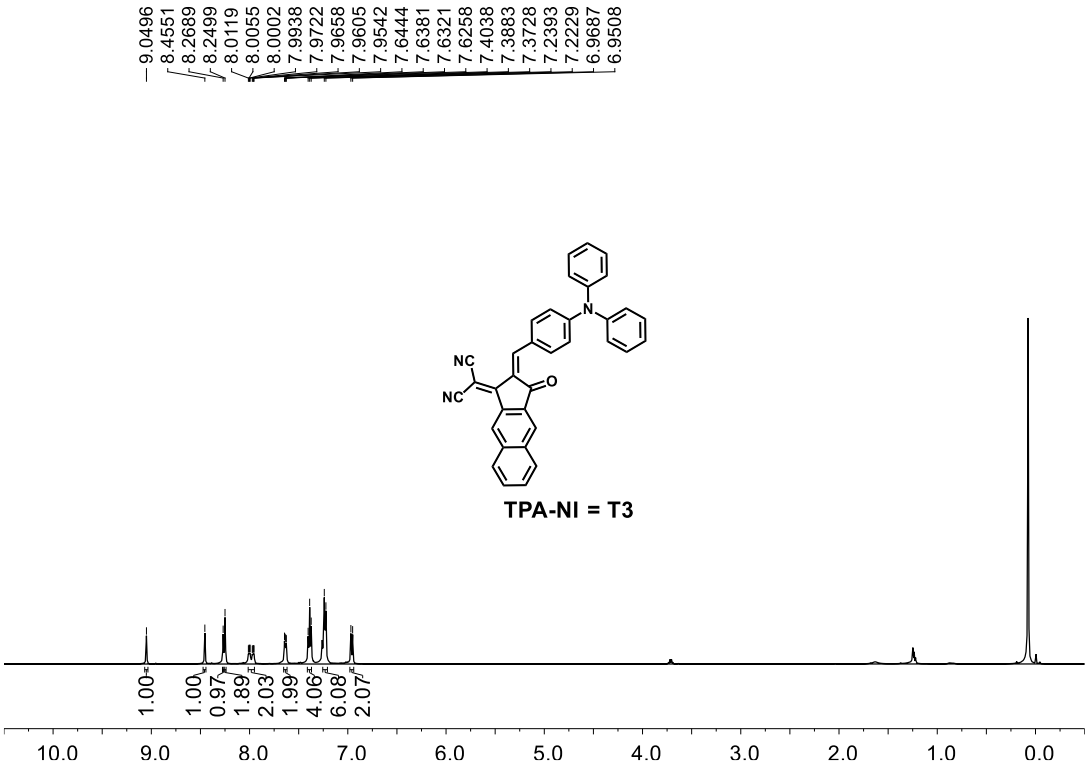

Figure S3 ^{1}H NMR spectrum of T3.

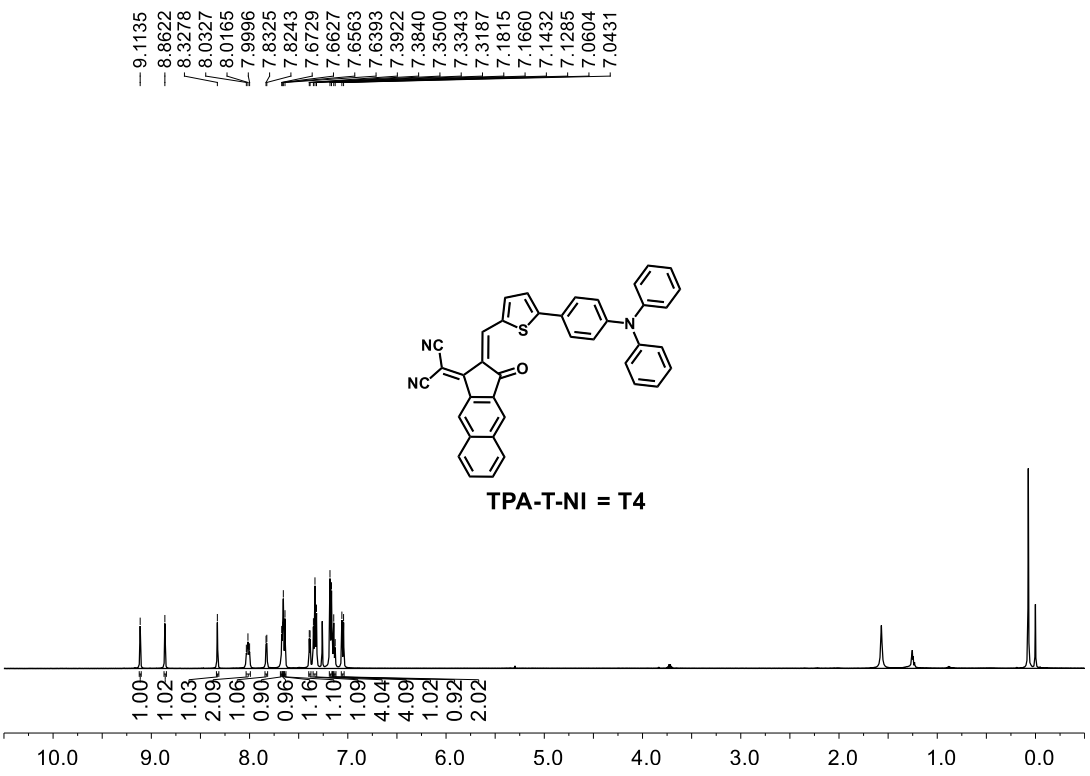

Figure S4 ^{1}H NMR spectrum of T4.

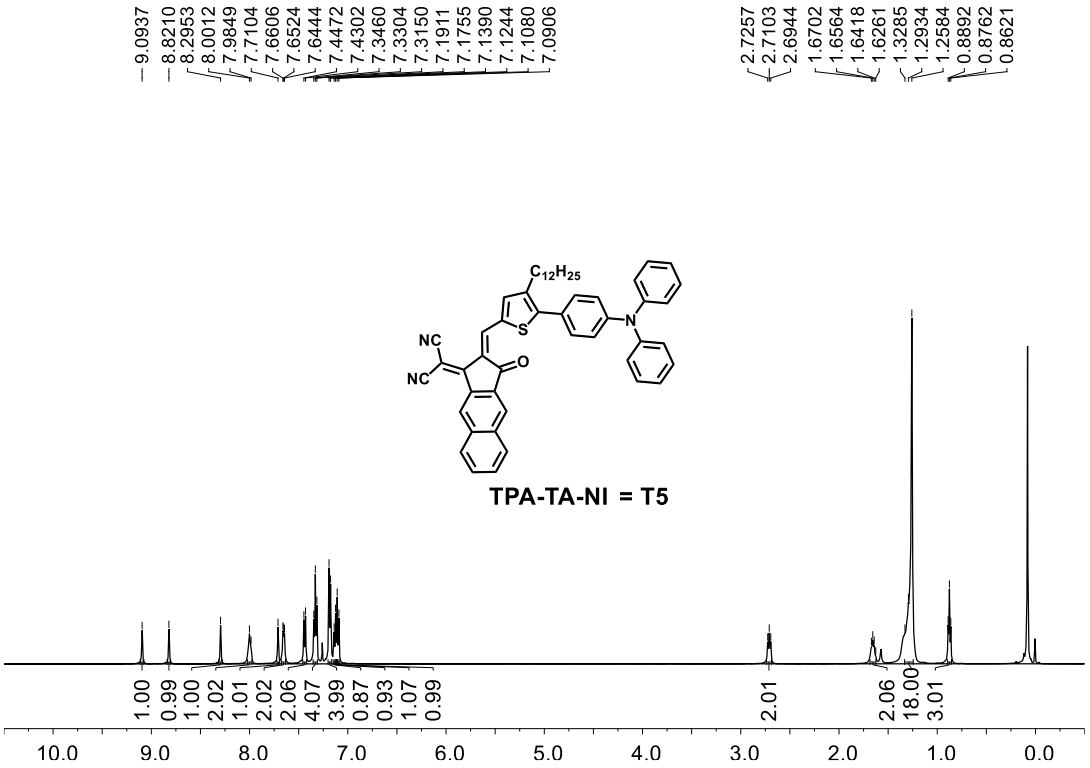

Figure S5 ^{1}H NMR spectrum of T5.

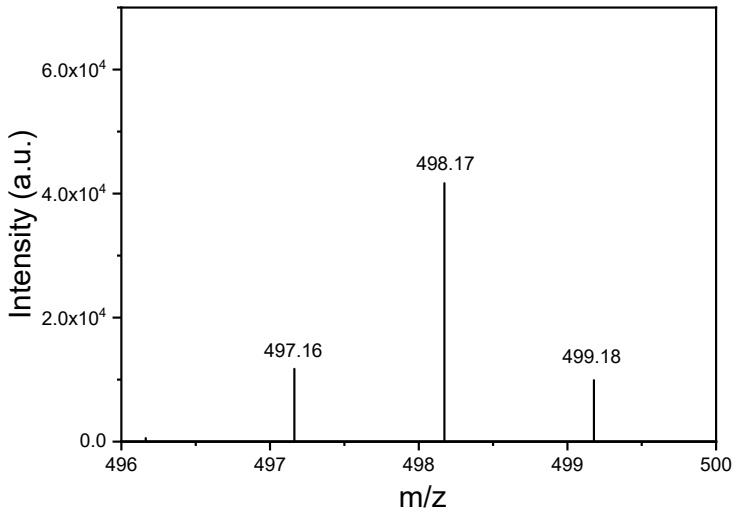

Figure S6 MALDI-TOF mass spectrum of T1.

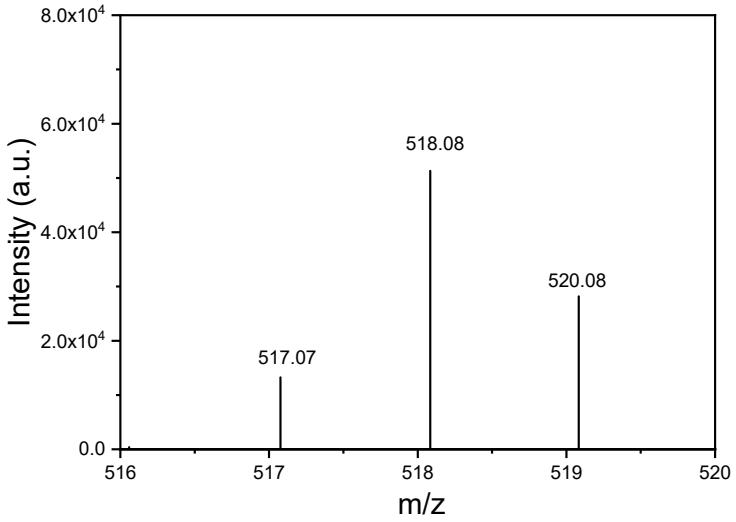

Figure S7 MALDI-TOF mass spectrum of T2.

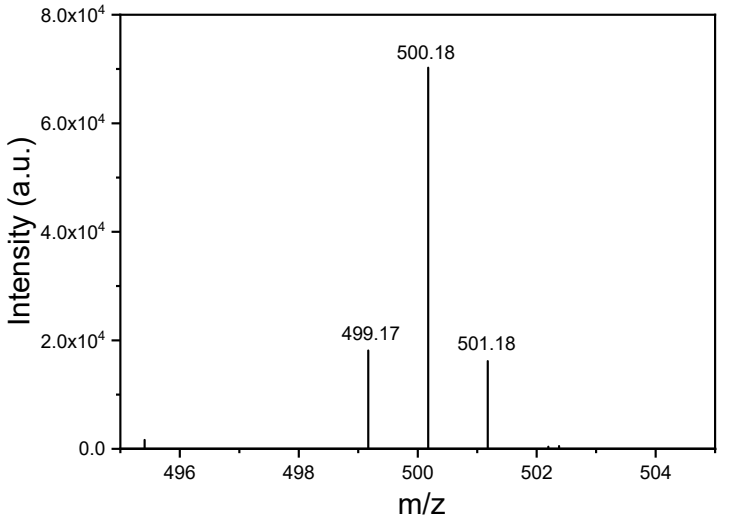

Figure S8 MALDI-TOF mass spectrum of T3.

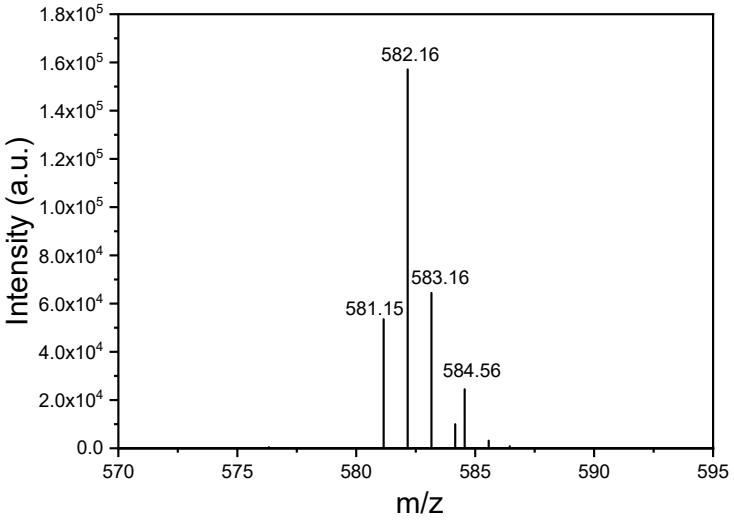

Figure S9 MALDI-TOF mass spectrum of T4.

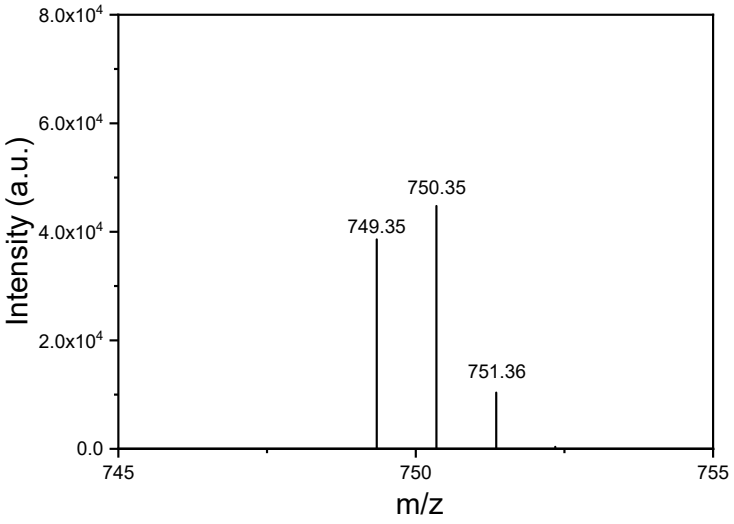

Figure S10 MALDI-TOF mass spectrum of T5.

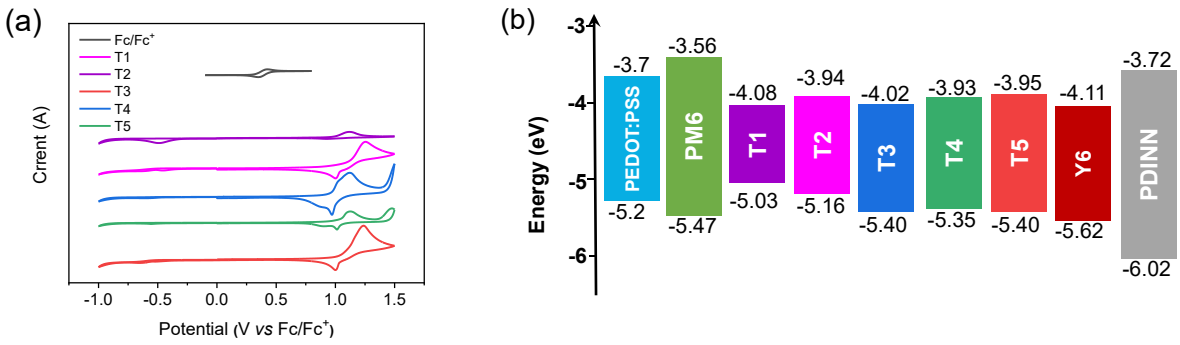

Figure S11 (a) Cyclic voltammograms of T1~T5 and Fc/Fc^{+}. (b) Energy levels diagram of materials used in this work.

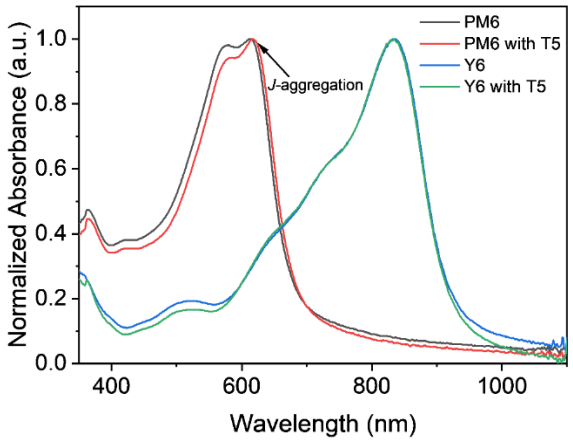

Figure S12 Normalized absorption spectra of PM6, PM6 with T5, Y6, and Y6 with T5 films.

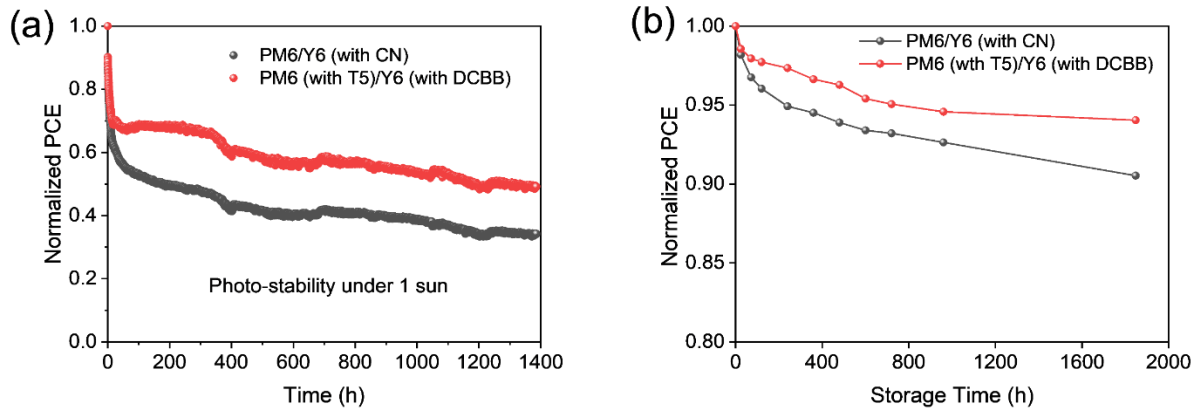

Figure S13 (a) Light stability of various OPVs with maximum power point (MPP) tracking under 1 sun illumination. (b) Storage stability of various OPVs without capsulation in the nitrogen glove box.

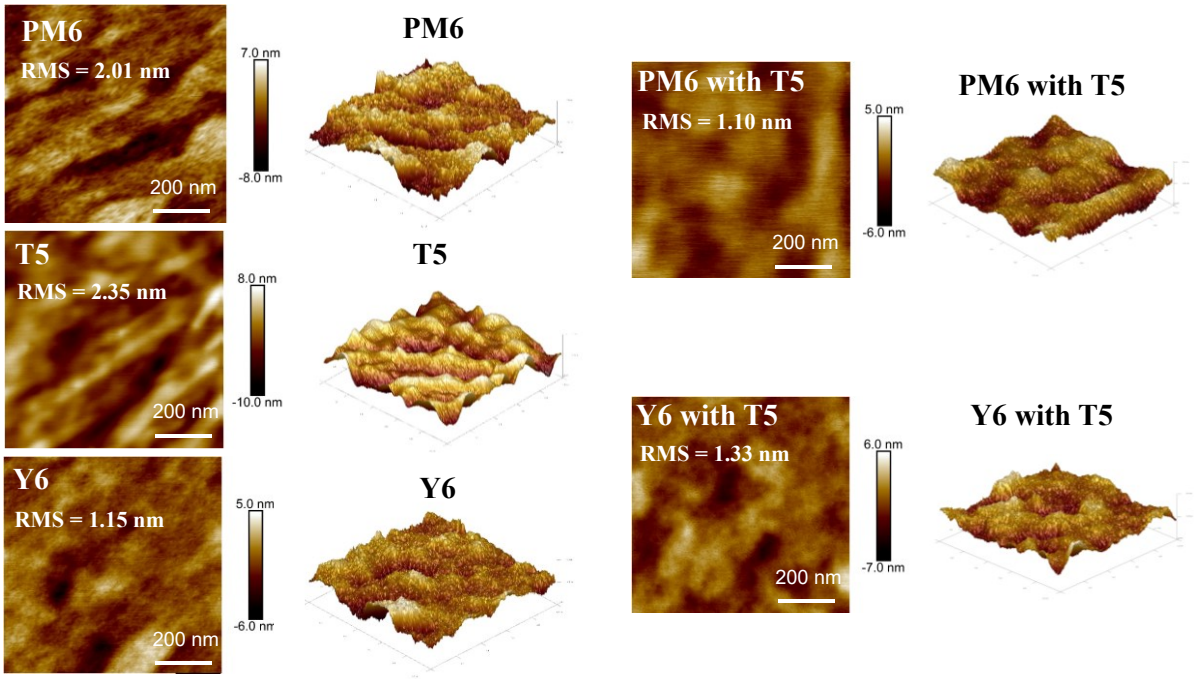

Figure S14 AFM height and 2D images of various neat films.

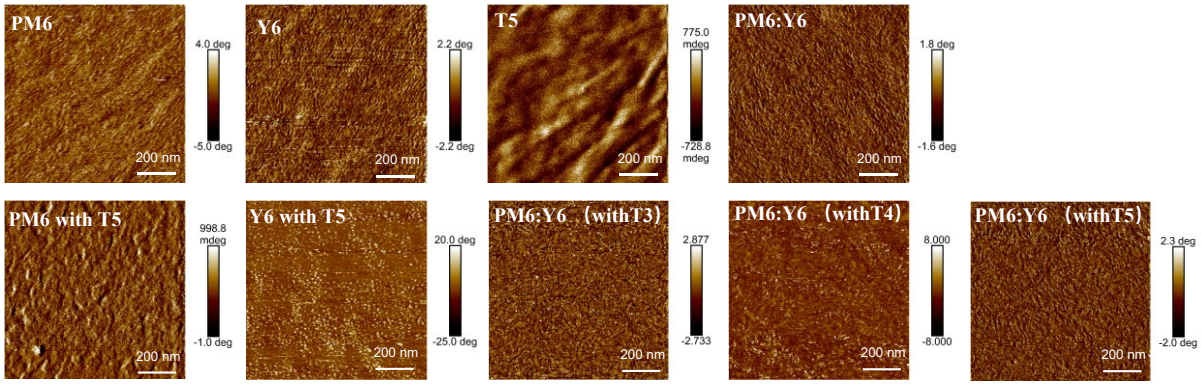

Figure S15 AFM phase images of various films.

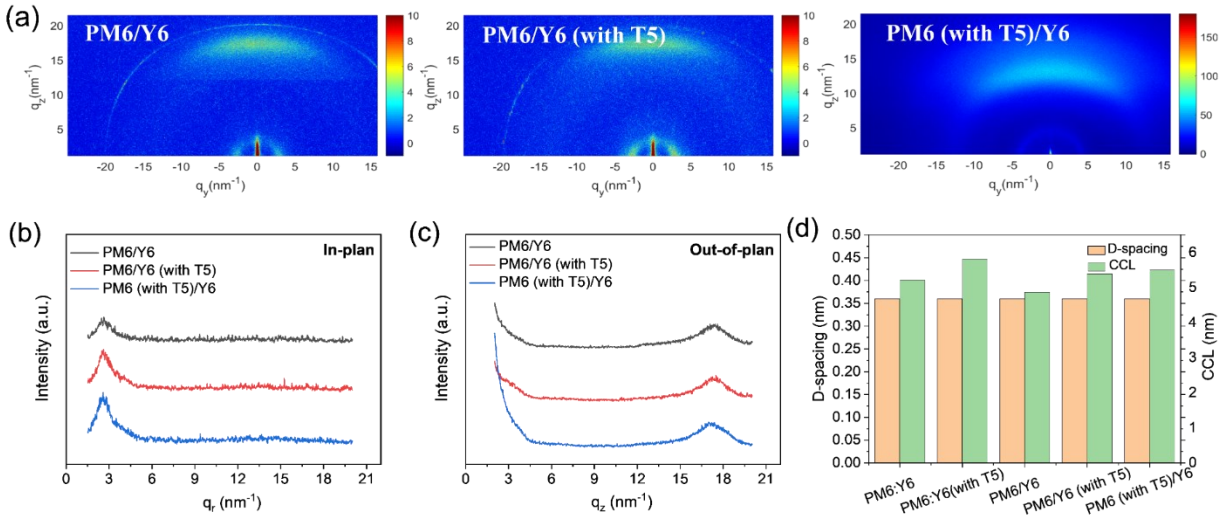

Figure S16 (a) 2D GIWAXS images of the LBL-type films. (b) 1D X-ray profiles of the corresponding films of in-plane and (c) out-of-plane directions. (d) D-spacing and CCL values along out-of-plane directions.

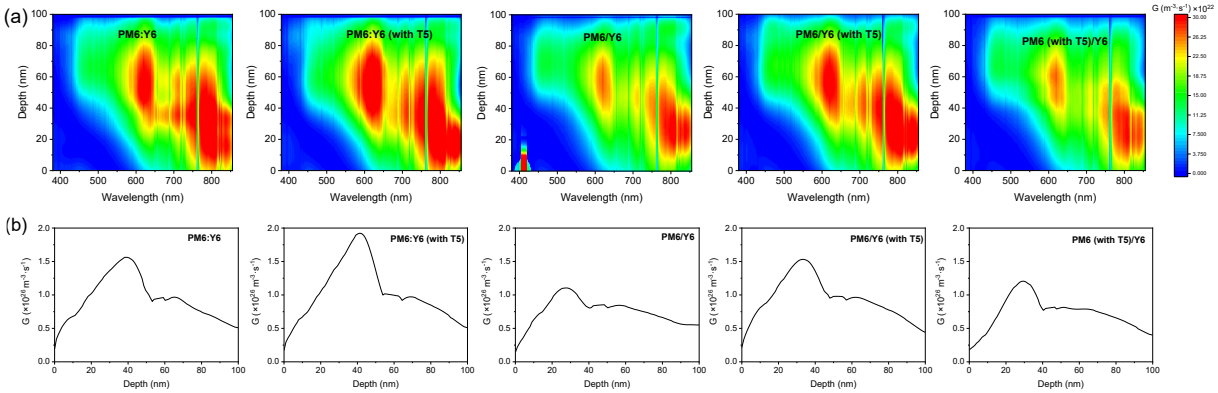

Figure S17 (a) Film-depth-dependent light absorption spectroscopy (FLAS) of various films. (b) Calculated exciton generation rate curves on the depth of the relevant films.

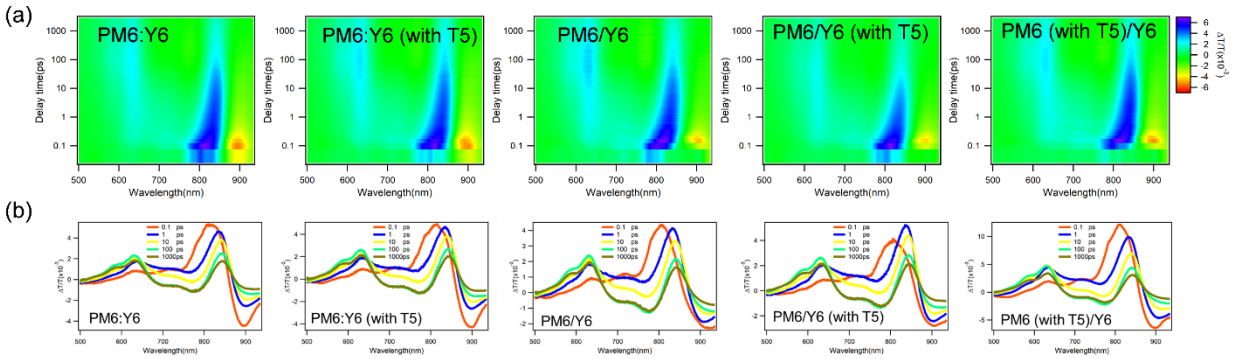

Figure S18 TA (a)color spectra and (b) curves of various blend films.

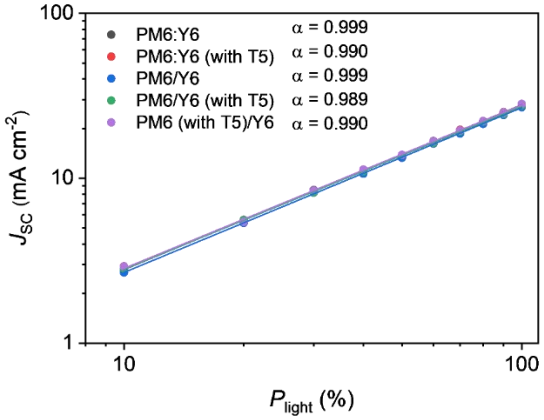

Figure S19 Dependence of J_{SC} on light intensity of the various devices.

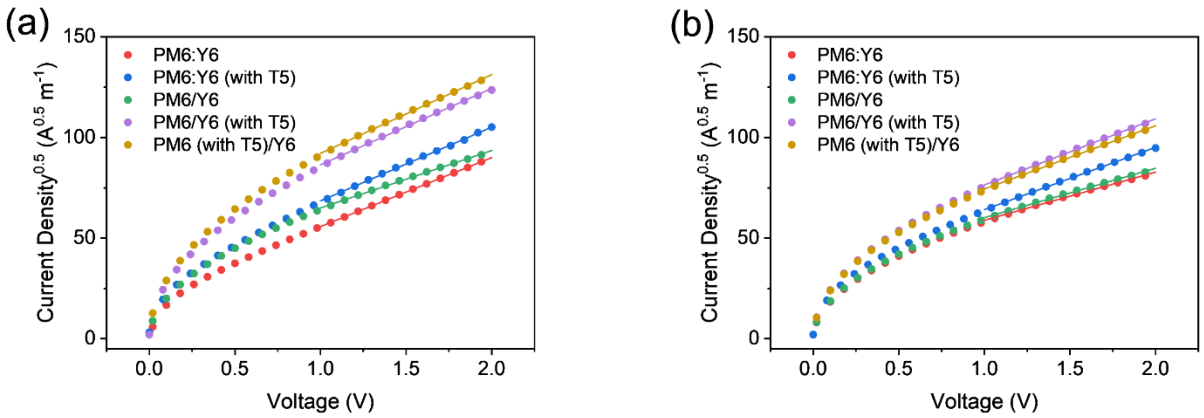

Figure S20 $J^{0.5}$-V curves of the (a) hole-only and (b) electron-only devices based on five blends.

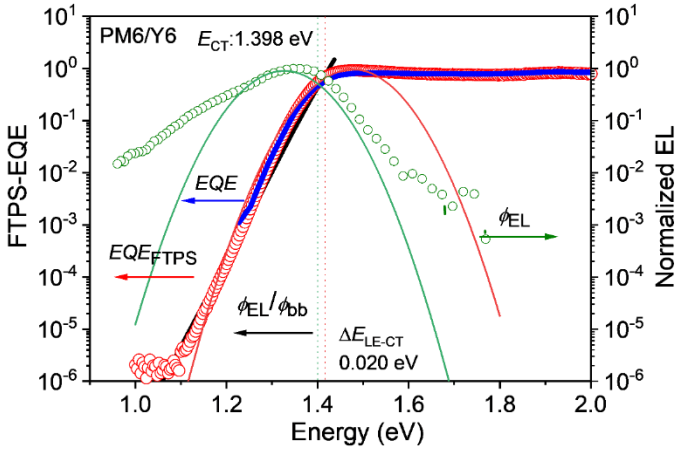

Figure S21 Gaussian fits of FTPS-EQE and EL curves via Marcus equation for devices based on PM6/Y6 film.

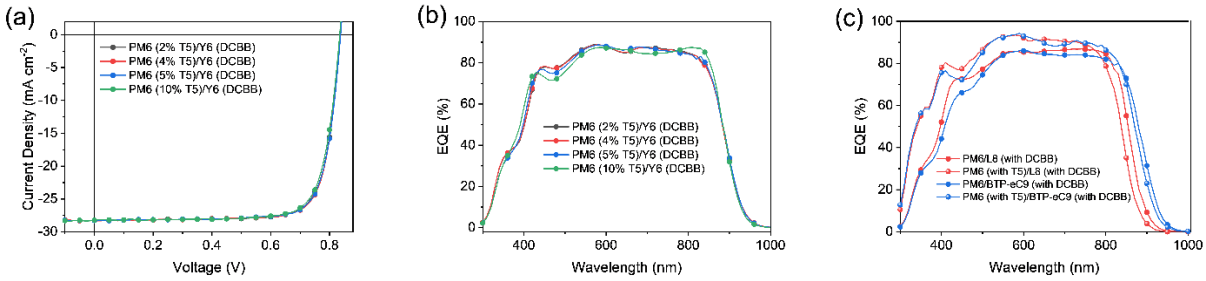

Figure S22 (a) *J-V* curve and (b) EQE curve of PM6/Y6-based devices fabricated with various ratio of T5 additive. (c) EQE curve of T5-optimized PM6/L8-BO and PM6/BTP-eC9 devices.

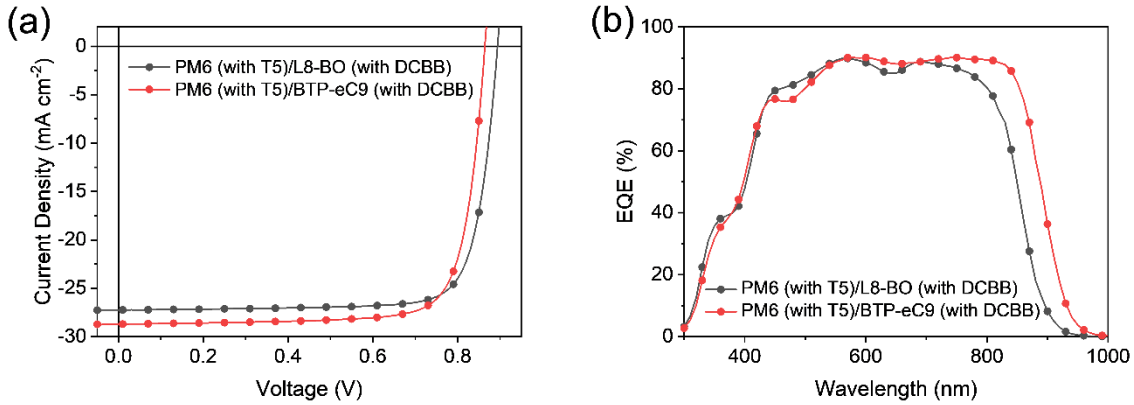

Figure S23 (a) *J-V* curves, and (b) EQE curves of T5-optimized PM6/L8-BO and PM6/BTP-eC9 devices fabricated in Prof. Chen's group at Zhejiang University.

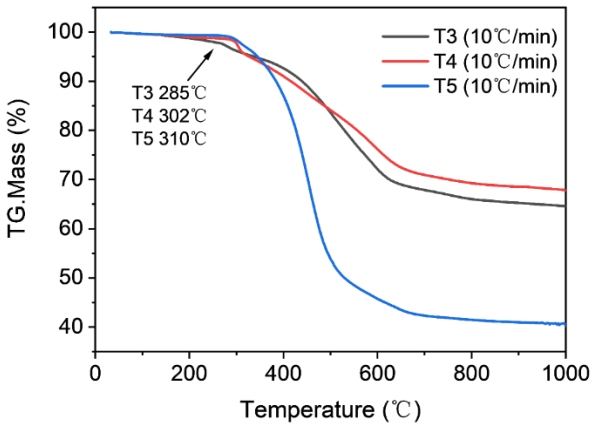

Figure S24 TG plots of three solid additives scanned at a rate of 10 °C/min.

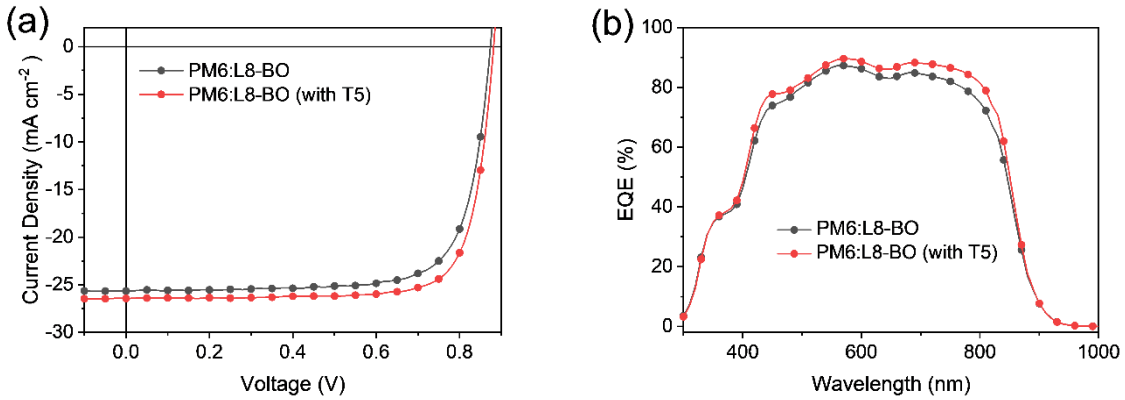

Figure S25 (a) *J-V* curves, and (b) EQE curves of PM6:L8-BO-based devices fabricated by toluene without and with T5 additive.

Supplementary Tables

Table S1. The photovoltaic parameters of the devices based on different additives and various device structures.

Active Layer	V_{OC} (V)	J_{SC} (mA cm^{-2})	J_{cal} [a] (mA cm^{-2})	FF (%)	PCE [b] (%)
PM6:Y6 (with T1)	0.843 (0.844 ± 0.002)	26.58 (25.04 ± 0.97)	25.41	70.87 (71.60 ± 0.56)	15.89 (15.14 ± 0.51)
PM6:Y6 (with T2)	0.848 (0.849 ± 0.003)	26.56 (25.91 ± 0.83)	25.54	70.31 (69.25 ± 0.89)	15.83 (15.24 ± 0.40)
PM6:Y6 (with T3)	0.846 (0.846 ± 0.002)	26.99 (26.72 ± 0.18)	25.91	70.79 (70.55 ± 0.41)	16.17 (15.97±0.13)
PM6:Y6 (with T4)	0.852 (0.851 ± 0.002)	26.98 (26.86 ± 0.19)	26.07	74.18 (73.88 ± 0.63)	17.08 (16.89 ± 0.16)

[a] Integrated current densities from EQE curves.
[b] Average PCEs from 10 devices.

Table S2 Summary of dispersion (γ^d) and polar (γ^p) components of surface tensions, surface tensions (γ), Flory-Huggins interaction parameters (χ) for various films.

Surface	γ^d (mN m^{-1})	γ^p (mN m^{-1})	γ (mN m^{-1})	χ^{D-A} [a]
PM6	37.93	0.03	37.96	/
Y6	38.49	0.95	39.44	/
PM6 with T1	34.12	0.01	34.13	/
PM6 with T2	34.32	0.09	34.41	/
PM6 with T3	37.30	0.00	37.30	/
PM6 with T4	37.05	0.02	37.08	/
PM6 with T5	34.93	0.05	34.98	/
T5	38.01	0.11	38.12	/
Y6 with T5	39.36	0.56	39.92	/
PM6:Y6	/	/	/	0.0141
PM6 (with T1):Y6	/	/	/	0.1919
PM6 (with T2):Y6	/	/	/	0.1716
PM6 (with T3):Y6	/	/	/	0.0298
PM6 (with T4):Y6	/	/	/	0.0366
PM6 (with T5):Y6	/	/	/	0.1341
PM6:T5	/	/	/	0.0002
Y6:T5	/	/	/	0.0113
PM6:Y6 (with T5)	/	/	/	0.0247

[a] The Flory-Huggins interaction parameter between the donor (D) and acceptor (A) is calculated through the equation of $\chi^{D-A} = (\sqrt{\gamma_D} - \sqrt{\gamma_A})^2$.

Table S3 Structure parameters of the various films with different incidence angles obtained from GIWAXS data.

Films	Position (nm^{-1})	FWHM (nm^{-1})	D-spacing (nm)	CCL (nm)
PM6:Y6	17.28	2.319	0.364	5.21
PM6:Y6 (with T3)	17.12	2.631	0.367	4.27
PM6:Y6 (with T4)	17.22	2.661	0.365	4.23
PM6:Y6 (with T5)	17.31	2.007	0.363	5.81
PM6/Y6	17.25	3.621	0.364	4.87
PM6/Y6 (with T5)	17.34	2.045	0.362	5.39
PM6 (with T5)/Y6	17.26	2.045	0.364	5.50

Table S4 Hole and electron mobilities of five blend films.

Sample	μ_h ($\times10^{-4}$ $cm^2 V^{-1} s^{-1}$)	μ_e ($\times10^{-4}$ $cm^2 V^{-1} s^{-1}$)	μ_h/μ_e
PM6:Y6	3.88 ± 0.68	1.91 ± 0.02	2.03
PM6:Y6 (with T5)	4.45 ± 0.88	3.21 ± 0.22	1.38
PM6/Y6	2.72 ± 0.02	2.01 ± 0.02	1.35
PM6/Y6 (with T5)	4.81 ± 0.24	3.61 ± 0.17	1.33
PM6 (with T5)/Y6	5.12 ± 0.11	3.32 ± 0.16	1.54

Table S5 Photovoltaic performance of OPVs processed with various ratio of T5.

Active Layer	V_{OC} (V)	J_{SC} (mA cm^{-2})	J_{cal} [a] (mA cm^{-2})	FF (%)	PCE [b] (%)
PM6 (with 2% T5)/ Y6 (with DCBB)	0.835 (0.834 ± 0.001)	28.21 (28.05 ± 0.17)	27.07	78.98 (78.72 ± 0.49)	18.63 (18.42 ± 0.13)
PM6 (with 4% T5)/ Y6 (with DCBB)	0.836 (0.839 ± 0.003)	28.28 (28.21 ± 0.15)	27.06	79.36 (78.72 ± 0.52)	18.78 (18.64 ± 0.11)
PM6 (with 5% T5)/ Y6 (with DCBB)	0.838 (0.837 ± 0.002)	28.28 (28.11 ± 0.15)	27.05	78.86 (78.59 ± 0.33)	18.67 (18.48 ± 0.07)
PM6 (with 10% T5)/ Y6 (with DCBB)	0.835 (0.835 ± 0.002)	28.23 (28.02 ± 0.20)	26.96	78.30 (78.43 ± 0.51)	18.44 (18.36 ± 0.07)

[a] Integrated current densities from EQE curves.
[b] Average PCEs from 10 devices.

Table S6 Photovoltaic performance of OPVs fabricated in Prof. Chen's group at Zhejiang University.

Active Layer	V_{OC} (V)	J_{SC} (mA cm^{-2})	J_{cal} [a] (mA cm-2)	FF (%)	PCE (%)
PM6 (with T5)/L8-BO (with DCBB)	0.894	27.25	25.59	80.26	19.55
PM6 (with T5)/BTP-eC9 (with DCBB)	0.864	28.72	27.96	79.00	19.61

[a] Integrated current densities from EQE curves.

Table S7 Photovoltaic performance of PM6:L8-BO-based devices fabricated by toluene without and with T5 additive.

Active Layer	V_{OC} (V)	J_{SC} (mA cm^{-2})	J_{cal} [a] (mA cm^{-2})	FF (%)	PCE [b] (%)
PM6:L8-BO	0.873 (0.870 ± 0.002)	25.64 (25.41 ± 0.24)	24.43	75.58 (75.77 ± 1.03)	16.90 (16.71 ± 0.14)
PM6:L8-BO (with T5)	0.881 (0.882 ± 0.003)	26.43 (26.33 ± 0.32)	25.54	78.50 (78.19 ± 0.49)	18.31 (18.19 ± 0.11)

[a] Integrated current densities from EQE curves.
[b] Average PCEs from 10 devices.

Table S8 Summary of the performance of large-area OPV devices and modules.

Total area (cm^2)	additive	V_{oc} (V)	J_{sc} (mA cm^{-2})	GFF(%)	FF (%)	PCE (%)	Ref.
1	CN	0.911	19.86	/	62.10	11.24	1
1	DIO	0.850	19.90	/	70.60	11.90	2
1	/	0.830	24.80	/	74.92	15.50	3
1.21	CN	0.939	21.71	/	72.12	14.70	4
5.4	CN	3.370	6.20	/	70.50	14.70	5
6.25	DIO	0.870	19.46	/	52.00	8.95	6
7	/	3.90	4.89	/	64.69	12.72	7
9	DIO	0.860	15.26	/	56.00	7.35	8
10.1	CN	0.810	23.56	/	66.00	12.60	9
10.8	DIO	2.760	5.29	/	67.00	9.80	10
11.52	/	3.200	6.41	91.4	57.85	11.86	11
12.6	CN	2.560	6.23	60.0	64.02	10.21	12
15	DIO	5.100	2.79	/	60.61	8.90	13
16	DIO	3.040	4.50	/	55.00	7.50	14
16.5	2-MN	0.734	2.69	/	70.10	13.84	15
18	/	11.60	0.99	/	55.00	6.30	16
18	/	4.810	3.60	70.6	66.80	11.60	17
18	/	5.110	3.89	70.6	72.50	14.40	17
18	/	0.898	24.19	95.4	66.33	14.41	our work
18.90	T5	0.911	25.17	95.4	70.77	16.23	our work
18.73	DIO	5.770	3.67	97.0	69.94	14.79	18
19.30	DIO	5.770	3.56	97.0	69.94	14.35	18
19.3	CN	6.104	3.55	/	71.43	15.48	19
19.3	CN	6.020	3.70	/	72.08	16.04	20
19.31	MT	5.945	3.66	/	72.39	15.74	21
19.34	CN	6.060	3.07	/	66.45	12.36	22
20.4	/	4.520	3.50	/	64.00	10.13	23
21	/	6.100	3.39	/	74.60	15.40	24
25	/	3.900	4.57	/	63.32	11.29	3
25	CN	9.824	1.84	96.0	73.54	13.27	25

25.2	DIB	6.010	3.42	/	70.17	14.42	26
28.82	DMN	12.850	1.36	93.8	72.48	12.64	27
31.50	DTBF	4.210	2.83	/	53.00	6.26	28
31.50	DPE	4.270	4.65	/	62.61	12.44	29
32.6	/	9.450	1.79	/	61.20	10.30	30
36	CN	10.020	2.01	/	70.81	14.26	31
55.5	DPE	11.470	1.29	/	63.00	9.32	32
66	AA	11.700	0.89	69.0	59.00	6.10	33
72.25	DIO	14.710	1.29	94.0	67.37	12.78	34

Reference:

1. Y.-F. Shen, J. Zhang, C. Tian, D. Qiu and Z. Wei, *Nano Res.*, **2023**, *16*, 13008-13013.
2. K. Wang, W. Li, X. Guo, Q. Zhu, Q. Fan, Q. Guo, W. Ma and M. Zhang, *Chem. Mater.*, **2021**, *33*, 5981-5990.
3. H. Li, S. Liu, X. Wu, Q. Qi, H. Zhang, X. Meng, X. Hu, L. Ye and Y. Chen, *Energy Environ. Sci.*, **2022**, *15*, 2130-2138.
4. J. Liu, J. Deng, Y. Zhu, X. Geng, L. Zhang, S. Y. Jeong, D. Zhou, H. Y. Woo, D. Chen, F. Wu and L. Chen, *Adv. Mater.*, **2023**, *35*, 2208008.
5. S. Park, S. H. Park, H. Jin, S. Yoon, H. Ahn, S. Shin, K. Kwak, S. Nah, E.-Y. Shin, J. H. Noh, B. K. Min and H. J. Son, *Nano Energy*, **2022**, *98*, 107187.
6. K. S. Wienhold, V. Körstgens, S. Grott, X. Jiang, M. Schwartzkopf, S. V. Roth and P. Müller-Buschbaum, *ACS Appl. Mater. Interfaces*, **2019**, *11*, 42313-42321.
7. J. Xue, H. Zhao, C. Zhao, L. Tang, Y. Wang, J. Xin, Z. Bi, K. Zhou and W. Ma, *Adv. Funct. Mater.*, **2023**, *33*, 2303403.
8. Y. Han, X. Chen, J. Wei, G. Ji, C. Wang, W. Zhao, J. Lai, W. Zha, Z. Li, L. Yan, H. Gu, Q. Luo, Q. Chen, L. Chen, J. Hou, W. Su and C.-Q. Ma, *Adv. Sci.*, **2019**, *6*, 1901490.
9. F. Qin, L. Sun, H. Chen, Y. Liu, X. Lu, W. Wang, T. Liu, X. Dong, P. Jiang, Y. Jiang, L. Wang and Y. Zhou, *Adv. Mater.*, **2021**, *33*, 2103017.
10. C.-Y. Tsai, Y.-H. Lin, Y.-M. Chang, J.-C. Kao, Y.-C. Liang, C.-C. Liu, J. Qiu, L. Wu, C.-Y. Liao, H.-S. Tan, Y.-C. Chao, S.-F. Horng, H.-W. Zan, H.-F. Meng and F. Li, *Sol. Energy Mater. Sol. Cells*, **2020**, *218*, 110762.
11. R. Sun, Q. Wu, J. Guo, T. Wang, Y. Wu, B. Qiu, Z. Luo, W. Yang, Z. Hu, J. Guo, M. Shi, C. Yang, F. Huang, Y. Li and J. Min, *Joule*, **2020**, *4*, 407-419.
12. W. Zhao, Y. Zhang, S. Zhang, S. Li, C. He and J. Hou, *J. Mater. Chem. C*, **2019**, *7*, 3206-3211.

13. X. Meng, L. Zhang, Y. Xie, X. Hu, Z. Xing, Z. Huang, C. Liu, L. Tan, W. Zhou, Y. Sun, W. Ma and Y. Chen, *Adv. Mater.*, **2019**, *31*, 1903649.
14. K. Zhang, Z. Chen, A. Armin, S. Dong, R. Xia, H.-L. Yip, S. Shoaee, F. Huang and Y. Cao, *Sol. RRL* **2018**, *2*, 1700169.
15. Y. Cai, C. Xie, Q. Li, C. Liu, J. Gao, M. H. Jee, J. Qiao, Y. Li, J. Song, X. Hao, H. Y. Woo, Z. Tang, Y. Zhou, C. Zhang, H. Huang and Y. Sun, *Adv. Mater.*, **2023**, *35*, 2208165.
16. L. Mao, B. Luo, L. Sun, S. Xiong, J. Fan, F. Qin, L. Hu, Y. Jiang, Z. Li and Y. Zhou, *Mater. Horiz.*, **2018**, *5*, 123-130.
17. S. Dong, T. Jia, K. Zhang, J. Jing and F. Huang, *Joule*, **2020**, *4*, 2004-2016.
18. J.-Y. Fan, Z.-X. Liu, J. Rao, K. Yan, Z. Chen, Y. Ran, B. Yan, J. Yao, G. Lu, H. Zhu, C.-Z. Li and H. Chen, *Adv. Mater.*, **2022**, *34*, 2110569.
19. T. Chen, X. Zheng, D. Wang, Y. Zhu, Y. Ouyang, J. Xue, M. Wang, S. Wang, W. Ma, C. Zhang, Z. Ma, S. Li, L. Zuo and H. Chen, *Adv. Mater.*, **2024**, *36*, 2308061.
20. D. Wang, Y. Li, G. Zhou, E. Gu, R. Xia, B. Yan, J. Yao, H. Zhu, X. Lu, H.-L. Yip, H. Chen and C.-Z. Li, *Energy Environ. Sci.*, **2022**, *15*, 2629-2637.
21. Z. Jia, J. Pan, X. Chen, Y. Li, T. Liu, H. Zhu, J. Yao, B. Yan and Y. Yang, *Energy Environ. Sci.*, **2024**, *17*, 3908-3916.
22. Z. Jia, Z. Chen, X. Chen, J. Yao, B. Yan, R. Sheng, H. Zhu and Y. Yang, *Photon. Res.*, **2021**, *9*, 324-330.
23. C.-Y. Liao, Y. Chen, C.-C. Lee, G. Wang, N.-W. Teng, C.-H. Lee, W.-L. Li, Y.-K. Chen, C.-H. Li, H.-L. Ho, P. H.-S. Tan, B. Wang, Y.-C. Huang, R. M. Young, M. R. Wasielewski, T. J. Marks, Y.-M. Chang and A. Facchetti, *Joule*, **2020**, *4*, 189-206.
24. Z. Zhong, S. Chen, J. Zhao, J. Xie, K. Zhang, T. Jia, C. Zhu, J. Jing, Y. Liang, L. Hong, S. Zhu, D. Ma and F. Huang, *Adv. Energy Mater.*, **2023**, *13*, 2302273.
25. A. Distler, C. J. Brabec and H.-J. Egelhaaf, *Prog. Photovolt. Res. Appl.*, **2021**, *29*, 24-31.
26. S. Zhang, H. Chen, P. Wang, S. Li, Z. Li, Y. Huang, J. Liu, Z. Yao, C. Li, X. Wan and Y. Chen, *Sol. RRL* **2023**, *7*, 2300029.
27. Y. Li, J. Wu, X. Yi, Z. Liu, H. Liu, Y. Fu, J. Liu and Z. Xie, *J. Mater. Chem. C*, **2023**, *11*, 13263-13273.
28. H. W. Cho, S. Y. Jeong, Z. Wu, H. Lim, W.-W. Park, W. Lee, J. V. Suman Krishna, O.-H. Kwon, J. Y. Kim and H. Y. Woo, *J. Mater. Chem. A*, **2023**, *11*, 7053-7065.
29. S. Rasool, J. W. Kim, H. W. Cho, Y.-J. Kim, D. C. Lee, C. B. Park, W. Lee, O.-H. Kwon, S. Cho and J. Y. Kim, *Adv. Energy Mater.*, **2023**, *13*, 2203452.

30. C.-Y. Liao, Y.-T. Hsiao, K.-W. Tsai, N.-W. Teng, W.-L. Li, J.-L. Wu, J.-C. Kao, C.-C. Lee, C.-M. Yang, H.-S. Tan, K.-H. Chung and Y.-M. Chang, *Sol. RRL* **2021**, *5*, 2000749.
31. H. Chen, R. Zhang, X. Chen, G. Zeng, L. Kobera, S. Abbrent, B. Zhang, W. Chen, G. Xu, J. Oh, S.-H. Kang, S. Chen, C. Yang, J. Brus, J. Hou, F. Gao, Y. Li and Y. Li, *Nat. Energy* **2021**, *6*, 1045-1053.
32. T. Lee, S. Oh, S. Rasool, C. E. Song, D. Kim, S. K. Lee, W. S. Shin and E. Lim, *J. Mater. Chem. A*, **2020**, *8*, 10318-10330.
33. O. A. Ibraikulov, J. Wang, N. Kamatham, B. Heinrich, S. Méry, M. Kohlstädt, U. Würfel, S. Ferry, N. Leclerc, T. Heiser and P. Lévêque, *Sol. RRL* **2019**, *3*, 1900273.
34. X. Kong, L. Zhan, S. Li, S. Yin, H. Qiu, Y. Fu, X. Lu, Z. Chen, H. Zhu, W. Fu and H. Chen, *Chem. Eng. J.*, **2023**, *473*, 145201.